Title
Investigation of Aquo and Chloro Complexes of UO{sub 2}{sup 2+}, NpO{sub 2}{sup +}, Np{sup 4+}, and Pu{sup 3+} by X-ray Absorption Fine Structure Spectroscopy

Journal
Inorganic Chemistry, 36(21)

Author
Allen, P.G.

Publication Date
1997-04-01

LBNL-40248
UC-401
Preprint

ERNEST ORLANDO LAWRENCE
BERKELEY NATIONAL LABORATORY

Investigation of Aquo and Chloro Complexes of UO_2^{2+}, NpO_2^{+}, Np^{4+}, and Pu^{3+} by X-ray Absorption Fine Structure Spectroscopy

P.G. Allen, J.J. Bucher, D.K. Shuh, N.M. Edelstein, and T. Reich
Chemical Sciences Division

April 1997
Submitted to
Inorganic Chemistry

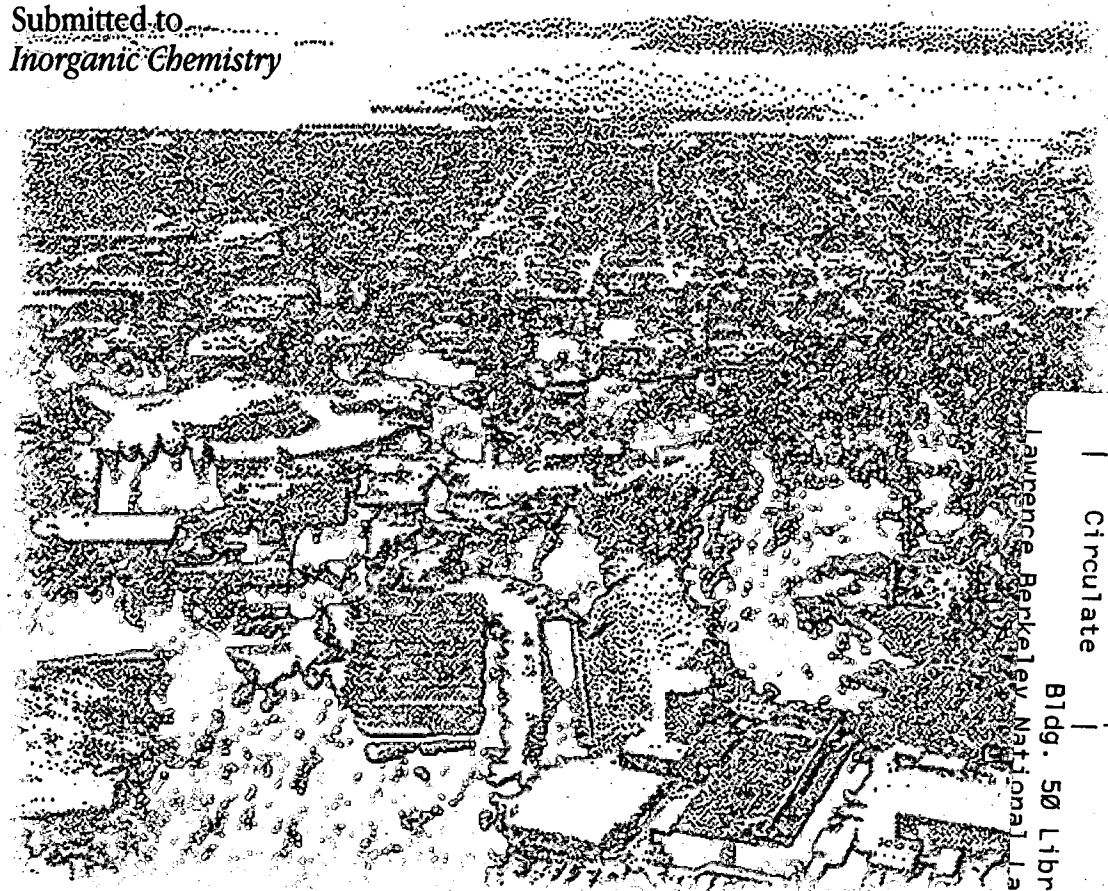

DISCLAIMER

LBNL-40248
UC-401

Investigation of Aquo and Chloro Complexes of UO_2^{2+}, NpO_2^{+}, Np^{4+}, and Pu^{3+} by X-ray Absorption Fine Structure Spectroscopy

P.G. Allen,[1] J.J. Bucher,[1] D.K. Shuh,[1] N.M. Edelstein,[1]
and T. Reich[2]

[1]Chemical Sciences Division
Ernest Orlando Lawrence Berkeley National Laboratory
University of California
Berkeley, California 94720

[2]Forschungszentrum Rossendorf e. V.
Institute für Radiochemie
Postfach 51 01 19
D-01314 Dresden, Germany

April 1997

This work was supported by the Director, Office of Energy Research, Office of Basic Energy Sciences, Chemical Sciences Division, of the U.S. Department of Energy under Contract No. DE-AC03-76SF00098.

Investigation of Aquo and Chloro Complexes of UO_2^{2+}, NpO_2^{+}, Np^{4+}, and Pu^{3+} by X-ray Absorption Fine Structure Spectroscopy

P. G. Allen,[1*] J. J. Bucher,[1] D. K. Shuh,[1] N. M. Edelstein,[1]

T. Reich[2]

[1]Chemical Sciences Division, Lawrence Berkeley National Laboratory, Berkeley, CA 94720

[2]Forschungszentrum Rossendorf e. V., Institute für Radiochemie, Postfach 51 01 19,

D-01314 Dresden, Germany.

Abstract

U, Np, and Pu $L_{II,III}$-edge x-ray absorption fine structure (XAFS) spectra were collected for the UO_2^{2+}, NpO_2^{+}, Np^{4+}, and Pu^{3+} ions as a function of chloride concentration in aqueous solution. At low chloride concentration, the hydration numbers and corresponding bond lengths for the different ions are: UO_2^{2+}, N = 5.3, R = 2.41 Å; NpO_2^{+}, N = 5.0, R = 2.50 Å; Np^{4+}, N = 11.2, R = 2.40 Å; and Pu^{3+}, N = 10.2, R = 2.51 Å. As the Cl^- concentration increases, inner sphere Cl^- complexation occurs resulting in a decrease in the hydration numbers and an expansion of the actinide–oxygen (water) bond lengths. The Pu^{3+} ion shows only a decrease in hydration number (40%) and no inner sphere Cl^- complexation for $[Cl^-] < 14$ M. For concentrations up to 10-14 M Cl^-, the average Cl^- coordination numbers and bond lengths are: UO_2^{2+}, N = 2.6, R = 2.73 Å; NpO_2^{+}, N = 1.0, R = 2.84 Å; Np^{4+}, N = 2.0, R = 2.61 Å. Structural changes are observed in the near-edge spectral region as shown by significant changes in the white line intensities upon Cl^- complexation. For ions with similar structures, i.e. Pu^{3+} and Np^{4+}, or the actinyl ions NpO_2^{+} and UO_2^{2+}, positive energy shifts are observed with increasing oxidation state. The ability to use XAFS speciation results to calculate equilibrium constants and the relationship of these results to previous studies is discussed.

Introduction

Chloride complexation studies of the actinide ions Ac^{3+}, Ac^{4+}, AcO_2^+, and AcO_2^{2+} (Ac = U, Np, or Pu) have been reported in several comprehensive reviews of thermodynamic data.[1-5] In general, these studies have employed a variety of analytical methods (solvent extraction, potentiometric titrations, ion exchange, etc.) to determine stability constants or most frequently, stability quotients, which can be used in conjunction with extrapolation models (i.e., specific-ion interaction[6] or Pitzer[7]) to calculate the principal species in solution for a given set of ionic conditions. The identification of the chemical species is important not only for understanding actinide separations and processing chemistry, but also provides information which is essential for predicting actinide transport in the environment,[8] particularly with respect to the safety assessment of proposed nuclear waste repositories.

Although a large amount of work has been published, considerable discrepancies exist concerning the nature of the actinide chloride interactions (inner sphere or outer sphere complexation), complex formation constants, and solution structure. Relatively good agreement is found for Cl^- complexation with the uranyl ion, UO_2^{2+}, where the log β_1 values for the formation of UO_2Cl^+ determined in 2 M (Cl^-, ClO_4^-) at 25 °C range from -0.06 to -0.15.[9-11] However for NpO_2^+, a value of log β_1 = -0.29 has been reported,[12] while another study determined that no complexation occurs in this system.[13] More recently, a zero ionic strength value of -0.29 for log β_1 was obtained, and based on spectroscopic evidence the NpO_2Cl complex formation was proposed to be outer-sphere.[14] The log β_1 values obtained for Np(IV) in 2 M ClO_4^- solutions are also somewhat uncertain, ranging from 0.04 at 20 °C to -0.28 at 25 °C.[15,16] Other studies indicate that the species $NpCl^{3+}$ predominates in solutions of 5 M HCl.[17] The same types of discrepancies are also found for Pu(III), with log β_1 values reported from -0.15 to -2.43.[18,19]

These data indicate that the chloride complexation with the actinide ions UO_2^{2+}, NpO_2^+, Np^{4+}, and Pu^{3+} is extremely weak. Since most of the research to date has been based on indirect analytical methods, the structures as well as the actual existence of these complexes in high ionic strength brines have not been directly confirmed. We have investigated the formation of chloride

complexes with the actinide ions UO_2^{2+}, NpO_2^{+}, Np^{4+}, and Pu^{3+} using x-ray absorption fine structure (XAFS) spectroscopy.[20] These species were chosen as representatives of the AcO_2^{2+}, AcO_2^{+}, Ac^{4+}, and Ac^{3+} ions due to their availability and stability. In this paper, the Cl^- concentration in aqueous solution is systematically varied, and XAFS is used to determine the structural changes that occur around the actinide core ion. Since XAFS spectroscopy directly determines the local structural environment for metal ions in solution, actinide chloro and aquo complexes that have been postulated in earlier work can be directly characterized.

Experimental Section

Solution and Sample Preparation. All sample preparations were done using the Actinide Chemistry Group facilities at the Lawrence Berkeley National Laboratory (LBNL). A.C.S. reagent grade anhydrous lithium chloride (Aldrich) and A.C.S. reagent grade conc. hydrochloric acid (J. T. Baker) were used as received. Analytical grade Dowex anion exchange resin, AG1-X8, 200-400 mesh, chloride form (Bio-Rad Labs.), with 3.2 milliequivalents per gram of resin exchange capacity was used. The resin was washed with a series of 1, 6, and 9 M HCl solutions until the eluant was clear. A final rinse with 0.1 M HCl was made before the resin was filtered to remove the excess liquid. Double-distilled deionized water was used for all solution preparations.

A 2.0 M stock solution of the UO_2^{2+} ion was prepared by weighing uranyl nitrate, $UO_2(NO_3)_2 \cdot 6\,H_2O$ (B & A, Allied Chemical & Dye Corp.). All lithium chloride solutions were prepared from a 0.001 M HCl solution. A 0.46 M stock solution of NpO_2^{+} was prepared by dissolving NpO_2 powder (^{237}Np) obtained from Los Alamos National Laboratory in 0.100 M HCl. The isotopic purity was determined by high resolution alpha spectroscopy using a surface barrier detector (Tennelec, ~20 keV resolution). In addition to ^{237}Np, the stock solution contained 0.26 mole percent ^{239}Pu and 0.0003 mole percent ^{241}Am. Stock solution concentrations were determined by comparing a 1:2000 dilution ^{237}Np platinum counting plate against an ^{241}Am standard (traceable to NBS). A plot of the apparent ^{237}Np concentration versus ^{241}Am counting

efficiency was made to allow extrapolation to "zero" efficiency in order to correct for the different geometries of isotope deposition on the counting plates.

Removal of the ^{239}Pu, ^{241}Am impurities, and the equilibrium ^{233}Pa daughter was accomplished by multiple extractions using 0.5 M TTA (thenoyltrifluoroacetone) in benzene followed with several benzene washes to remove the residual TTA. Alpha spectroscopy confirmed the removal of ^{239}Pu (which interferes with the Np XAFS data collection) and ^{241}Am to detection limits. A 0.1 M stock solution of the Np^{4+} ion was prepared from the NpO_2^+ solution by reduction to Np^{3+} using a Zn amalgam followed by air oxidation to Np^{4+}. The stock was maintained at 0.1 M HCl acidity. Similarly, a 0.035 M Pu^{3+} stock solution was prepared from a Pu^{4+} solution by Zn amalgam reduction. The plutonium isotope used was ^{242}Pu and the principal transuranic impurity was ^{241}Am (0.05 mole percent).

Most of the solutions were mixed into 10 mm diameter plastic centrifuge tubes in an ambient atmosphere glovebox. The final actinide and chloride concentrations are summarized in Table 1. LiCl was used in the NpO_2^+ solution preparations to avoid disproportionation and in the UO_2^{2+} and Pu^{3+} solutions when higher Cl^- activities were desired. Smaller plastic tubes (5 mm dia.) and sample volumes were used at high chloride concentrations to minimize the attenuation and background scattering from the Cl^- ions in the solutions. The Dowex resin samples were prepared by allowing the mixture to equilibrate and removing most of the residual solution leaving a wet paste. The solutions were sealed in the tubes by melting the caps directly onto the plastic body with a soldering iron. The outsides of the samples were surveyed to insure that no detectable alpha radiation was present. Having established the integrity of the primary containers, each sample was placed within two additional layers of containment consisting of two heat-sealed polyethylene bags. The triply contained, inspected, and certified samples were then transported to the Stanford Synchrotron Radiation Laboratory (SSRL). The samples (5-10 at any given time) were mounted on an aluminum frame which was placed inside a quaternary containment box with 0.17 mm polycarbonate x-ray windows. The box was placed inside the x-ray hutch on a specially designed sample positioner. The hutch as well as the sample mounting and storage areas were equipped

with LBNL continuous air monitors, alpha radiation detectors, and alarms for safety purposes. Access to the samples was carefully controlled at all times.

XAFS Data Acquisition and Analysis. Uranium, neptunium, and plutonium $L_{II,III}$ edge x-ray absorption spectra were collected at SSRL on wiggler beamline 4-1 under normal ring operating conditions (3.0 GeV, 50-100 mA). Energy scans of the polychromatic x-ray beam were obtained using a Si (220) double-crystal monochromator and a vertical slit width of 0.5 mm. The higher order harmonic content of the beam was rejected by detuning the crystals in the monochromator so that the incident flux was reduced to 50% of its maximum at the scan ending energy. The samples containing UO_2^{2+} in 1-10 M HCl and the UO_2^{2+}:Dowex sample were measured in transmission mode using Ar-filled ionization chambers. All of the neptunium, plutonium, and the remaining uranium solutions were measured in fluorescence mode using a Ge solid state detector developed at Lawrence Berkeley National Laboratory.[21] The detector was operated at ~200 kHz per channel and the spectra were corrected for detector deadtime using a 2 μsec time constant.

XAFS data reduction, including treatment of both the extended x-ray absorption fine structure (EXAFS) and the x-ray absorption near-edge structure (XANES) spectral regions, was performed by standard methods reviewed elsewhere[20] using the suite of programs EXAFSPAK developed by G. George of SSRL. Typically, three XAFS scans (transmission or fluorescence) were collected from each sample at ambient temperature, and the results were averaged. The spectra were energy calibrated by simultaneously measuring the absorption spectrum for the reference sample UO_2, NpO_2, or PuO_2 as appropriate. The energies of the first inflection points for the reference sample absorption edges, E_r, were defined at 17166.0 eV (U L_{III}), 17606.2 eV (Np L_{III}), and 22258.0 (Pu L_{II}). Pu XAFS data were acquired at the L_{II}-edge to avoid monochromator crystal glitches encountered at k = 8 $Å^{-1}$ above the L_{III}-edge. The EXAFS threshold energies, E_0, were defined as 17185 eV, 17625 eV, and 22275 eV for the U, Np, and Pu samples, respectively. Nonlinear least-squares curve-fitting for the raw k^3-weighted EXAFS data and spectral deconvolutions of the XANES data were done using the EXAFSPAK programs.

The EXAFS data were fit using theoretical phases and amplitudes calculated from the program FEFF6 of Rehr *et al.*[22] All of the interactions were modeled using single scattering (SS) and multiple scattering paths (MS) derived from the model compounds $UO_2Cl_2 \cdot H_2O$,[23] $CsNpO_2Cl_2 \cdot H_2O$,[24] Cs_2UCl_6 (i.e., $NpCl_6^{2-}$ or $PuCl_6^{2-}$),[25] and the hypothetical clusters $Np(H_20)_{12}^{4+}$ and $Pu(H_20)_{10}^{3+}$. For the actinyl complex spectra, a total of four paths were employed: SS Ac–O_{ax} (axial), SS Ac–O_{eq} (equatorial), SS Ac–Cl, and MS O–Ac–O (4 legged path). Since the MS path occurs at exactly twice the Ac–O_{ax} distance, it is included as a fixed parameter directly linked to the floating Ac–O_{ax} parameters.[26,27] Fits to the Np^{4+} and Pu^{3+} data utilized two paths: SS Ac–O and SS Ac–Cl. An initial series of fits were done on the UO_2^{2+}:0.0 M HCl and the UO_2^{2+}:Dowex data to establish accurate Debye-Waller factors, σ, for the Ac–O_{eq} and Ac–Cl shells. Similarly, reasonable values of σ were obtained for the Np^{4+} O and Cl^- interactions using the Np^{4+}:1.0 M HCl and Np^{4+}:Dowex data. All the subsequent fits were performed using fixed σ values for these shells, and a fixed coordination number of N=2 for the Ac–O_{ax} shell. S_0^2, the amplitude reduction factor, was held fixed at 0.9 in each of the fits. The shift in threshold energy, ΔE_0, was allowed to vary as a global parameter in each of the fits (i.e., the same ΔE_O was used for each shell). Consequently the fits were highly constrained which avoided N and σ correlation problems and established more consistently the changes in coordination as a function of Cl^- concentration.[28,29]

Results and Discussion

UO_2^{2+} EXAFS. Figure 1 shows the raw k^3-weighted EXAFS data and the corresponding Fourier transforms (FT) for UO_2^{2+} in aqueous solution as a function of chloride concentration. The theoretical curve fits are also shown and the structural results are summarized in Table 2. The FT represents a pseudo-radial distribution function and the peaks are shifted to lower R values as a result of the phase shifts associated with the absorber-scatterer interactions (~0.2-0.5 Å). In the absence of Cl^-, the FT of the free uranyl spectrum shows two peaks which arise from the presence of 2 O_{ax} at 1.76 Å and ~5 O_{eq} at 2.41 Å. This is consistent with the

structural result obtained previously for the fully hydrated uranyl ion.[30] The spectrum of the UO_2^{2+}:Dowex sample shows a different pattern with a much larger FT peak occurring at a higher *R*-value than the O_{eq} peak for the hydrated uranyl ion. The curve fits indicate that the complex anion $UO_2Cl_4^{2-}$, analogous to that in $Cs_2UO_2Cl_4$ solid,[31] is formed in the Dowex resin with 4.2 Cl^- at 2.67 Å and no evidence for O_{eq} (no improvement in the fit by including O_{eq}). An inspection of the 1-14 M Cl^- data shows that a structural transformation is occurring in the equatorial region, and initial curve-fits to these spectra indicated the structural changes could be fit primarily by changes in the O_{eq} and Cl^- coordination numbers. Therefore in subsequent fits, the values of σ for the O_{eq} and Cl^- shells were fixed to those obtained from the $UO_2(H_2O)_5^{2+}$ and $UO_2Cl_4^{2-}$ spectra.

From 1 M to14 M Cl^-, the curve fits demonstrate a systematic replacement of O_{eq} by Cl^-. As the Cl^- concentration increases, the Cl^- coordination number N_{Cl^-} increases from 0.3 to 2.6, the O_{eq} coordination number $N_{O_{eq}}$ decreases from 5.0 to 1.9, and bond lengths for the O_{eq} shell lengthen from 2.41 Å to 2.52 Å. It is important to note that the curve-fitting results represent an average of all possible species present in these solutions, i.e., $UO_2(H_2O)_5^{2+}$, $UO_2(H_2O)_xCl^+$, or $UO_2(H_2O)_xCl_2$. The standard deviations for *R* and *N*, and the *F*-value ratios obtained from the endpoint fits are also shown in Table 2.[32] Based on these results, the presence of Cl^- at 4 M is confirmed. However, employing 95% confidence limits shows that this is not the case for the 1 and 2 M spectra. While it appears that there is a trend in the *F*-ratios, and an increase in precision gained by measuring multiple spectra in EXAFS has been demonstrated,[28,29] the fitting results of ~0.3 ± 0.3 Cl^- obtained by the inclusion of Cl^- in the 1 and 2 M data are at the noise level. One of the important results obtained is the presence of 2.6 ± 0.3 Cl^- in 14 M Cl^-. A value of $N_{Cl^-} > 2$ even with the effects of averaging, necessitates the presence of a species having the form $UO_2(H_2O)_xCl_3^-$. These data also suggest that as the molar ratio of H_2O/UO_2^{2+} decreases, the concomitant decrease in $N_{O_{eq}}$ is mitigated through simple Cl^- replacement-an effect which at this level is indistinguishable from that of a decrease in the activity of H_2O.[30] The structural effect of Cl^- replacement is to lengthen the U–O_{eq} bonds.

NpO_2^+ EXAFS. The raw k^3-weighted EXAFS data and Fourier transforms for NpO_2^+ are shown in Figure 2 along with the corresponding fits as a function of the Cl^- concentration. Although there is a higher noise level in these data relative to the uranyl spectra, the important features are clearly observed in the FTs. The FT for NpO_2^+ in 3 M Cl^- shows two peaks analogous to the O_{ax} and O_{eq} peaks for UO_2^{2+} without Cl^-. As the Cl^- concentration is increased from 6 to 10 M, an additional peak appears immediately to the high *R* side of the O_{eq} peak. This peak correlates both in position and magnitude to the Cl^- peak for UO_2^{2+} in 4 M Cl^-. Spectral changes are observed in the k-space data in Figure 2a around k= 6–7 $Å^{-1}$ (also see Figure 1a). Since the NpO_2^+ ion has a similar structure to that of UO_2^{2+}, curve-fits were done using the same σ values for the O_{eq} and Cl^- shells that were used in the UO_2^{2+} fits (Table 3).

In 3 M Cl^-, the Np(V) environment consists of 2 O_{ax} at 1.85 Å and 5 O_{eq} at 2.50 Å.[33] This structure is nearly identical to that of the fully hydrated UO_2^{2+} ion with the exception of longer bond lengths which are expected for the larger Np(V) ion. For higher Cl^- concentration, N_{Cl^-} increases from 0 to ~1, $N_{O_{eq}}$ decreases from ~5 to 4, and the O_{eq} bond lengths expand from 2.50 Å to 2.53 Å. As was done for the fits to the uranyl EXAFS, *F*-value ratios were determined along with standard deviations for *R* and *N*. However, since the NpO_2^+ EXAFS data possess a significant amount of high frequency noise, the *F*-value ratios reported were derived from fits to Fourier-filtered data to remove the noise.[34] The factor of two improvement achieved by including Cl^- in the fits of the 7-10 M Cl^- spectra shows that Cl^- is present in the equatorial region of the NpO_2^+ ion for these solutions. The relative magnitudes and positions of the different contributions to the fit of the 10 M spectrum are shown in Figure 3 for comparison. Although the uncertainty in N_{Cl^-} is relatively large, the Np–O_{eq} and Np–Cl bond lengths are in agreement with those reported by XRD for the solid, $CsNpO_2Cl_2 \cdot H_2O$.[24] These data show that the Cl^- replacement in NpO_2^+ is substantially weaker than in UO_2^{2+}, yet the nature of the complexation is the same (i.e., the water molecules move out, and the Cl^- ligation is inner-sphere).

Np^{4+} EXAFS. Figure 4 shows the raw k^3-weighted EXAFS data and the corresponding FTs for Np^{4+} as a function of chloride concentration. The curve-fitting results are

summarized in Table 4. The FT for Np^{4+} in 1 M Cl^- shows a single prominent peak which is fit by a single shell of ~11 O at 2.40 Å. This is consistent with the first shell structure of $Pu(NO_3)_2(H_20)_x^{2+}$ which is ~11-coordinate and has an average Pu–O bond length of 2.41 Å.[35] The Np–O bond lengths in $Np(H_20)_{11}^{4+}$ are significantly longer than the 2.35 Å value for 8-coordinate Np in NpO_2.[36] The spectrum of the Np^{4+}:Dowex sample yields a much larger FT peak occurring at a higher *R*-value than the O peak in the 1 M spectrum. Curve fitting yields ~ 6 Cl^- at 2.61 Å suggesting that the complex anion $NpCl_6^{2-}$ is formed in the Dowex resin. This structure and the bond lengths agree with those found previously for the octahedral $AcCl_6^{2-}$ units present in Cs_2UCl_6[25] and Cs_2PuCl_6.[37] The FTs in Figure 4b show that there are no structural changes occurring up to 5-6 M Cl^-, whereas from 6 to 10 M Cl^-, there is a clear shift to higher *R* as well as a broadening in the FT peak. Since the origin of these changes was determined by curve-fitting to be replacement of O by Cl^- in the coordination sphere (i.e., changes in N_O and N_{Cl^-}), the values of σ were fixed to those obtained from the $Np(H_2O)_{11}^{4+}$ and $NpCl_6^{2-}$ fits.

As described earlier, the standard deviations for *N* and the *F*-value ratios were evaluated to justify the inclusion of Cl^- (or O) in the fit.[34] Going from 5 M to 10 M Cl^-, the curve fits demonstrate a systematic replacement of O by Cl^-. As the Cl^- concentration increases, N_{Cl^-} increases from 0 to 2.0, and N_O decreases from 10.3 to 7.7. Since the level of fit improvement increases from 5 to 10 M Cl^-, and the 95% confidence level for N_{Cl^-} is ± 0.36, the value of N_{Cl^-} = 0.6 obtained for the 6 M data confirms the presence of Cl^- in the inner sphere at this concentration. These results represent an average of all possible species, and a value of N_{Cl^-} ~ 2 in 10 M Cl^- indicates that multichloro complexes are formed, i.e., $Np(H_2O)_xCl_y^{4-y}$, with $y \geq 2$. Additionally, the Np^{4+} data show the same structural effect observed in the actinyl chloride complexes in that the O neighbors from water molecules move out as Cl^- enters the first coordination sphere.

Pu^{3+} EXAFS. In contrast to the behavior of the UO_2^{2+}, NpO_2^+, and Np^{4+} ions, Pu^{3+} showed no evidence for the formation of inner sphere chloro complexes up to a Cl^- concentration of 12.3 M. The Pu L_{II}-edge EXAFS data presented in Figure 5 display a trend of decreasing amplitude with no shifts to higher *R* as a function of increasing Cl^- concentration. The curve-

fitting results in Table 5 show that in dilute Cl^-, the Pu^{3+} environment consists of ~10 O at 2.51 Å. This result agrees well with the average first shell Ln^{3+} coordination in $Pr(OH)_3$ and $Nd(NO_3)_3 \cdot 6H_2O$, which consist respectively of 9 O at 2.53 Å and 10 O at 2.56 Å.[38,39] In 12.3 M Cl^-, the coordination is reduced to 6 O neighbors at 2.50 Å. The decrease in N_O likely reflects the diminished activity of water at 12.3 M LiCl where γ_{H_2O}~ 0.175.[40]

UO_2^{2+}, NpO_2^+, Np^{4+}, and Pu^{3+} XANES. The XANES spectra provide another diagnostic tool for studying the changes in these solutions as a function of Cl^- concentration. Figure 6 shows representative L_{III}-edge spectra for UO_2^{2+}, NpO_2^+, and Np^{4+}, and L_{II}-edge spectra for Pu^{3+} with varying amounts of Cl^- ligation as determined by EXAFS. Since the U, Np, and Pu data were calibrated against their respective Ac(IV)O_2 powder XANES spectra (nearly identical),[41] the data in Figure 6 are displayed on a relative energy scale which allows for direct comparison between the Np, U, and Pu spectra. The $L_{II,III}$ absorption edges of the actinides arise from the formally allowed $2p_{1/2,3/2} \rightarrow 6d$ electronic transitions, and changes in the L_{III} XANES for Ac(III), Ac(IV), AcO_2^+, and AcO_2^{2+} ions have been discussed in detail.[41-45] The $L_{II,III}$ XANES for Ac(III, IV) compounds are characterized by a single relatively intense absorption peak or "white line" whereas the XANES for actinyl compounds typically display a less intense absorption peak (relative to AcO_2) with a MS resonance occurring ~15 eV past the main peak.

A visual inspection of Figure 6 shows that the relative positions of the edges for the various oxidation states are in agreement with those shown previously for U and Np compounds.[44,45] There are positive energy shifts going from Pu^{3+} to Np^{4+} and from NpO_2^+ to UO_2^{2+} reflecting an increase in relative binding energy associated with an increase in positive charge on the actinide ion. However, there appears to be a negative energy shift from Np^{4+} to NpO_2^+.[45] The shifts in white line (WL) positions for the aquo ions were determined using a peak deconvolution procedure similar to ones employed earlier for actinide L_{III}-edges.[43-46] Relative to the WL positions of the Ac(IV)O_2 reference samples, the aquo ion WL shifts are -3.9 eV for Pu^{3+},[47] +0.7 eV for Np^{4+}, -1.3 eV for NpO_2^+, and + 1.4 eV for UO_2^{2+}. The negative WL shift observed going from Np^{4+} to NpO_2^+ may result from a combination of structural[43] and electronic[45] effects, which can be

difficult to distinguish from each other. For example, recent theoretical modeling using FEFF6 has shown that much of the structure associated with the L_{III} XANES of UO_2 and UO_2^{2+} including the MS resonance in UO_2^{2+} (previously interpreted as a split WL)[45] can be accurately modeled using SS and MS paths which contribute to the EXAFS portion, $\chi(k)$, of the total absorption, $\mu(E)$.[48-50] The anomalous WL shifts for the actinyl spectra relative to Np^{4+} may also reflect the diminished positive charge density on the Ac atoms in the actinyl groups that arises due to the close proximity of the axial oxygen atoms. Indeed, electronic structure simulations and thermodynamic measurements have determined effective charges of 2.2 on Np in NpO_2^+ and 3.2 for U in UO_2^{2+}.[51,52]

The effects of Cl^- replacement on the Np^{4+} XANES in Figure 6 are clearly observed. As N_{Cl^-} increases, the WL loses intensity, and the low-k EXAFS signal at ~40 eV progressively changes its position and amplitude. For Pu^{3+}, a decrease in N_O without any Cl^- ligation causes a similar reduction in the WL intensity. Increasing the Cl^- ligation around UO_2^{2+} also results in a decreased WL intensity and increased absorption in the vicinity of the MS resonance above the edge. The NpO_2^+ XANES data show a trend analogous to that of UO_2^{2+}. The XANES data for NpO_2^+ in 10 M Cl^- and for UO_2^{2+} in 4 M Cl^- are shown in Figure 6 for direct comparison since their EXAFS curve fits gave the same structural result of $N_{O_{eq}} \sim 1$. Even though the changes in the NpO_2^+ XANES are relatively small, they occur in the same direction as those in the UO_2^{2+} XANES. Preliminary modeling of these data suggests that at least part of the changes observed here are due to changes in $\chi(k)$ that result from either Cl^- replacement of O or a decrease in N_O as was found for Pu^{3+}. However, careful theoretical modeling is required to quantify these effects as well as the origin of the anomalous edge shifts mentioned above. Regardless of the assignments which are beyond the scope of this work, these spectra show dramatic sensitivity to changes in the local structure and help to corroborate the results obtained from the EXAFS analysis. Given that the signal to noise ratio is substantially larger in the XANES region relative to the EXAFS region, the enhanced XANES sensitivity should be useful for future work on more dilute systems where EXAFS data is unattainable.

Concluding Remarks

This work has directly measured the formation of chloro complexes with the actinide ions Pu^{3+}, Np^{4+}, NpO_2^+, and UO_2^{2+}, and characterized the structural parameters associated with the O and Cl^- ligation in these systems using XAFS spectroscopy. Based on the Cl^- concentrations that were required to form monochloro complexes with each ion, the log β_1 values for the reaction, $Ac^{x+} + Cl^- \leftrightarrow AcCl^{x-1}$, where Ac = Pu^{3+}, Np^{4+}, NpO_2^+, or UO_2^{2+} should follow the trend $UO_2^{2+} > Np^{4+} \approx NpO_2^+ >> Pu^{3+}$. It is further possible to estimate the formation quotients by viewing the behavior of N_{Cl^-} vs [Cl^-] as a type of titration curve, where [ ] refers to the molarity M. If we assume that monochloro complex formation is the principal process occurring early in the titration (i.e. $N_{Cl^-} < 1$), the EXAFS data will depict an average of the two species that are present. When $N_{Cl^-} = 0.5$, $[Ac^{x+}] = [AcCl^{x-1}]$ and $\beta_1 = 1/[Cl^-]$. This calculation gives log β_1 = -0.48, -0.78, and -0.85 for UO_2^{2+}, Np^{4+}, and NpO_2^+, respectively. These molar concentration equilibrium quotients apply only for the ionic strength at which they were determined. If we assume equal activities for the Ac^{x+} and $AcCl^{x-1}$ species, or alternatively that their activities tend to compensate each other, then it is possible to calculate an equilibrium constant which includes the Cl^- activity by using $\beta_1^0 = 1/\gamma_{Cl^-} m_{Cl^-}$, where γ_{Cl^-} is the mean molal activity coefficient and m_{Cl^-} is molality.[53] This correction gives log β_1^0 = -0.65, -1.47, and -1.65 for UO_2^{2+}, Np^{4+}, and NpO_2^+, respectively.

A comparison of the log β_1 and log β_1^0 values calculated here with those given earlier[9-19] shows that there is good agreement in the relative trend among the different ions. However, the values determined by EXAFS are significantly lower than those obtained in earlier measurements. The origin of these discrepancies is not clear. However for formation constants determined by ion exchange chromatography, the EXAFS results described in this work show that the ion exchange medium dramatically alters the formation of chloride complexes. Thus, the species $UO_2Cl_4^{2-}$ and $NpCl_6^{2-}$ were observed to readily form within the Dowex resin, but were not observed as principal species in the aqueous chloride solutions. Solvent extraction methods may suffer from similar

perturbations since the actinide ions under study are in contact with an organic solvent and extractant and numerous assumptions have to be made on the behavior of the extractant and the distribution of species among the different phases. In fact in a recent study on NpO_2^+ complexation with Cl^-, it was suggested that the chloro complex formation may be over-estimated by solvent extraction methods when compared to visible/NIR spectroscopic results.[14] In this case, the presence of outer sphere complexation or ion pairs was proposed to explain the discrepancy. From the EXAFS results presented in this work, only inner sphere complex formation was determined. Detection of outer sphere Cl^- complexation by EXAFS should yield a substantially weaker signal due to the lack of direct bonding and the increased distance, yet recent EXAFS results on aqueous solutions of Cr(III) and Zn(II) have suggested that detection of outer sphere O (~3.9 Å) or Cl^- (~4.3 Å) complexation is possible.[54] For solutions of $LaCl_3$, XRD indicates the presence of a $La(H_2O)_9Cl_2^+$ complex where the La–Cl interactions are outer sphere at ~5 Å.[55] Although the Fourier transforms in Figures 1, 2, 4, and 5 show no interactions at $R \geq 4$ Å which would indicate the presence of ordered shells of more distant neighbors, this does not exclude the possibility of outer sphere Cl^- complexation being present in these systems. The presence of 1-2 Cl^- ions at 5.0 Å may be undetectable by EXAFS, and studies with heavier halides or measurements at the halide absorption edges are needed to investigate these possibilities further.

Acknowledgment

This work was supported by the Director, Office of Energy Research, Office of Basic Energy Sciences, Chemical Sciences Division of the U. S. Department of Energy under Contract No. DE-AC03-76SF00098. This work was done (partially) at SSRL which is operated by the Department of Energy, Division of Chemical Sciences. The authors also acknowledge the efforts of the EH&S personnel from LBNL, SLAC, and SSRL.

References

(1) Grenthe, I.; Fuger, J.; Konings, R. J. M.; Lemire, R. J.; Muller, A. B.; Nguyen-Trung, C.; Wanner, H. *Chemical Thermodynamics of Uranium*; Wanner, H., Forest, I., eds.; Elsevier Science Publishers: Amsterdam, 1992; p. 193.

(2) Ahrland, S. in *The Chemistry of the Actinide Elements Vol. 2*; Katz, J. J., Seaborg, G. T., Morss, L. R., eds.; Chapman and Hall: New York, 1986; p. 1498.

(3) Fuger, J. in *Plutonium Chemistry* , ACS Symp. Ser. 216, Carnall, W. T., Choppin, G. R., eds.; American Chemical Society: Washington DC, 1983; p. 74.

(4) Degischer, G.; Choppin, G. R. in *Gmelin Handbuch der Anorganische Chemie, Transuranium*, Part D1: Chemie in Lösung, (Suppl. Vol. 20); Springer-Verlag : Berlin, 1975; p. 129.

(5) a) Sillén, L. G.; Martell, A. E. *Stability Constants of Metal-Ion Complexes,* Spec. Publ. No. 17; The Chemical Society: London, 1964. b) *Ibid*, Spec. Publ. No. 25; 1971.

(6) a) Scatchard, G. *Chem. Rev.* **1936**, *19*, 309. b) Ciavatta, L. *Ann. Chim.* (Rome) **1980**, 551.

(7) Pitzer, K. S. in *Activity Coefficients in Electrolyte Solutions,* Pitzer, K. S. ed.; CRC Press: Boca Raton Fl., 1991; pp 75-154.

(8) a)*Chemistry and Migration Behaviour of Actinides and Fission Products in the Geosphere:* Proceedings of the Fourth International Conference, Charleston, SC 1993. *Radiochimica Acta*, **1994**, *66/67*, 1-833. b) *Chemistry and Migration Behaviour of Actinides and Fission Products in the Geosphere:* Proceedings of the Fifth International Conference, Saint Malo, France 1995. *Radiochimica Acta* **1996**, *74*, 1-327.

(9) Day, R. A.; Powers, R. M. *J. Am. Chem. Soc.* **1954**, *76*, 3895.

(10) Bednarczyk, L.; Fidelis, I. *J. Radioanal. Nucl. Chem.* **1978**, *45*, 325.

(11) Awasthi, S. P.; Sundaresan, M. *Indian J. Chem.* **1981**, *20A*, 378.

(12) Gainar, I.; Sykes, K. W.; *J. Chem. Soc.* **1964**, 4452.

(13) Danesi, P. R.; Chiarizia, R.; Scibona, G.; D'Alessandro, G. *J. Inorg. Nucl. Chem.* **1974**, *36*, 2396.

(14) Neck, V.; Fanghänel, Th.; Rudolph, G.; Kim, J. I. *Radiochimica Acta* **1995**, *69*, 39-47.

(15) Shilin, I. V.; Nazarov, V. K. *Radiokhimiya* **1966**, *8*, 514.

(16) Sykes, K. W.; Taylor, B. L. *Proc. Seventh International Conference on Coordination Chemistry* **1962**, p. 31.

(17) Marcus Y. *Coord. Chem. Rev.* **1967**, *2*, 195.

(18) Connick, R. E.; McVey, W. H. *J. Am. Chem. Soc.* **1953**, *75*, 474.

(19) Shiloh, M.; Marcus, Y. *J. Inorg. Nucl. Chem.* **1966**, *28*, 2725.

(20) Prins, R.; Koningsberger, D. E. *X-ray Absorption: Principles, Applications, Techniques for EXAFS, SEXAFS, and XANES*; Wiley-Interscience: New York, 1988.

(21) Bucher, J. J.; Edelstein, N. M.; Osborne, K. P.; Shuh, D. K.; Madden, N.; Luke, P.; Pehl, D.; Cork, C.; Malone, D.; Allen, P. G. *SRI '95 Conference Proceedings, Rev. Sci. Instr.* 67, 1996. 1.

(22) Rehr, J. J.; Mustre de Leon, J.; Zabinsky, S.; Albers, R. C. *Phys. Rev. B* **1991**, *44*, 4146.

(23) Taylor, J. C.; Wilson, P. W. *Acta Crystallogr.* **1974**, *B30*, 169-175.

(24) Tomilin, S. V.; Yu, F.; Volkov, F.; Melkaya, R. F.; Spiryakov, V. I.; Kapshukov, I. I. *Soviet Radiochemistry* **1986**, *28*, 634-639.

(25) Schleid, T.; Meyer, G.; Morss, L. R. *J. Less-Common Met.* **1972**, *132*, 69-77.

(26) Allen, P. G.; Bucher, J. J.; Clark, D. L.; Edelstein, N. M.; Ekberg, S. A.; Gohdes, J. W.; Hudson, E. A.; Kaltsoyannis, N.; Lukens, W. W.; Neu, M. P.; Palmer, P. D.; Reich. T.; Shuh, D. K.; Tait, C. D.; Zwick, B. D. *Inorg. Chem.*, **1995**, *34*, 4797.

(27) Allen, P. G.; Shuh, D. K.; Bucher, J. J.; Edelstein, N. M.; Reich. T.; Denecke, M. A.; Nitsche, H. *Inorg. Chem.*, **1996**, *35*, 784.

(28). Allen, P. G.; Conradson, S. D.; Wilson, M.; Gottesfeld, S.; Raistrick, I. D.; Valerio, J.; Lovato, M. *Electrochim. Acta* **1994**, *39*, 2415-2418.

(29) Allen, P. G.; Conradson, S. D.; Wilson, M.; Gottesfeld, S.; Raistrick, I. D.; Valerio, J.; Lovato, M. *J. Electroanal. Chem.* **1995**, *384*, 99-103.

(30) Åberg, M.; Ferri, D.; Glaser, J.; Grenthe, I. *Inorg. Chem.* **1983**, *22*, 3986-3989.

(31) Hall, D.; Rae, A. D.; Waters, T. N. *Acta Crystallogr.* **1966**, *20*, 160-162.

(32) F is a goodness of fit parameter defined as $F = \Sigma k^6(\text{data - fit})^2 / (N_{pts} - N_{var})$ where N_{pts} is the number of data points and N_{var} is the number of floating variables. The ratio of F-values obtained with and without the inclusion of a Cl^- (or O) shell of atoms is used here to quantify the fit improvement with Cl^- (or O) in the endpoint spectra (i.e., Cl^- detection limits in 0, 1, 2, 4 M HCl, and O detection limits in the Dowex sample).

(33) Combes, J. M.; Chisholm-Brause, C. J.; Brown, G. E., Jr.; Parks, G. A.; Conradson, S. D.; Eller, P. G.; Triay, I. R.; Hobart, D. E.; Meijer, A. *Environ. Sci. Technol.* **1992**, *26*, 376-382.

(34) The data were Fourier-filtered over the ranges k=1-12 $Å^{-1}$ and R=0.2-3.2 Å, and the filltered fits gave results that were nearly identical to those obtained from the raw data fits. The value for N_{pts} used to calculate the F-values is estimated by $2\Delta k\Delta R/\pi$.

(35) Allen, P. G.; Veirs, D. K.; Conradson, S. D.; Smith, C. A.; Marsh, S. F. *Inorg. Chem.* **1996**, *35*, 2841-2845.

(36) Zachariasen, W. H. Natl. Nuclear Energy Ser., Div. IV **1949**, *14B*, Transuranium Elements, Pt. II, 1489-1491.

(37) Zachariasen, W. H. *Acta Crystallogr.* **1948**, *1*, 268-269.

(38) Mullica, D. F.; Milligan, W. O.; Beall, G. W. *J. Inorg. Nucl. Chem.* **1979**, *41*, 525.

(39) Rogers, D. J.; Taylor, N. J.; Toogood, G. E. *Acta Crystallogr.* **1983**, *C39*, 939-941.

(40) Gazith, M. *Molal Osmotic Coefficients and Water Activities for Various Electrolytes.* IA-1009 (Israel AEC), 1965.

(41) Kalkowski, G.; Kaindl, G.; Bertram, S.; Schmiester, G.; Rebizant, J.; Spirlet, J. C.; Vogt, O. *Solid State Comm.* **1987**, *64*, 193-196.

(42) Farges, F.; Ponader, C.W.; Calas, G.; Brown, G.E., Jr. *Geochim. Cosmochim. Acta* **1992**, *56*, 4205.

(43) Petiau, J.; Calas, G.; Petitmaire, D.; Bianconi, A.; Benfatto, M.; Marcelli, A. *Phys. Rev. B* **1986**, *34*, 7350.

(44) Kalkowski, G.; Kaindl, G.; Brewer, W.D.; Krone, W. *Phys. Rev. B* **1987**, *35*, 2667.

(45) Bertram, S.; Kaindl, G.; Jové, J.; Pagès, M.; Gal, J. *Phys. Rev. Lett.* **1989**, *63*, 2680.

(46) Edge fits were done using EXAFSPAK, which treats the main absorption peak and other resonances as pseudo-Voigt peaks (mixture of Lorenztian and Gaussian shapes), and the discontinuous edge step function as the integral of a pseudo-Voigt function. The Ac(III, IV) spectra were fit using one peak plus the step function, while the actinyl XANES fits included a second peak to fit the MS resonance.

(47) XANES measurements performed for the Pu^{3+} aquo ion at the L_{III}-edge gave a WL shift of -3.7 eV relative to PuO_2.

(48) Hudson, E. A., Rehr, J. J., Bucher, J. J. *Phys. Rev. B* **1995**, *52*, 13815.

(49) Allen, P. G.; Shuh, D. K.; Bucher, J. J.; Edelstein, N. M.; Palmer, C. E-A.; Marquez, L. N.; Hudson, E. A.; Silva, R. J.; Nguyen, S. N. *Radiochim. Acta.* **1996**, *75*, 47-53.

(50) Hudson, E. A.; Allen, P. G.; Terminello, L. J.; Denecke, M.; Reich. T. *Phys. Rev. B* **1996**, *54*, 156.

(51) Denning, R. G. in *Structure and Bonding* , Vol. 79; Springer-Verlag : Berlin, 1992, p. 215.

(52) Choppin, G. R.; Rao, L. F. *Radiochim. Acta.* **1984**, *75*, 47-53.

(53) Gazith, M. *Activity Coefficients of Various Electrolytes. Molal and Molar Concentrations.* IA-1004 (Israel AEC), 1965.

(54) a) Díaz-Moreno, Sofía; Muñoz-Páez, A.; Martínez, J. M.; Pappalardo, R. R.; Marcos, E. S. *J. Am Chem. Soc.* **1996**, *118*, 12654-12664. b) Muñoz-Páez, A.; Pappalardo, R. R.; Marcos, E. S. *J. Am Chem. Soc.* **1995**, *117*, 11710-11720.

(55) Grigoriew, H.; Siekierski, S. *J. Phys. Chem.* **1993**, *97*, 5400-5402.

Table 1. Summary of Solution Preparations.

Actinde Ion	$[Ac^{x+}]$, M	Medium	$[Cl^-]$, M	Path length (mm)	Mode[a]
UO_2^{2+}	0.1	H_2O	0.0	10	T
	0.1	HCl	1.0	10	T
	0.1	HCl	2.0	10	T
	0.1	HCl	4.0	10	T
	0.1	HCl	6.0	10	T
	0.1	HCl	8.0	10	T
	0.1	HCl	10.0	10	T
	0.04	LiCl	12.0	5	F
	0.04	LiCl	14.0	5	F
	0.02	Dowex/HCl	10.0	10	T
NpO_2^+	0.005	LiCl	3.0	10	F
	0.005	LiCl	4.0	10	F
	0.005	LiCl	5.0	10	F
	0.005	LiCl	6.0	10	F
	0.005	LiCl	7.0	10	F
	0.005	LiCl	8.0	10	F
	0.005	LiCl	9.0	10	F
	0.005	LiCl	10.0	10	F
Np^{4+}	0.005	HCl	1.0	10	F
	0.005	HCl	2.0	10	F
	0.005	HCl	3.0	10	F
	0.005	HCl	4.0	10	F
	0.005	HCl	5.0	10	F
	0.005	HCl	6.0	10	F
	0.005	HCl	8.0	10	F
	0.005	HCl	10.0	10	F
	0.005	Dowex/HCl	10.0	10	F
Pu^{3+}	0.020	LiCl	0.01	10	F
	0.004	LiCl	7.0	5	F
	0.004	LiCl	8.7	5	F
	0.004	LiCl	10.5	5	F
	0.004	LiCl	12.3	5	F

a. Samples were measured in transmission (T) or fluorescence (F) mode.

Table 2. EXAFS Structural Parameters for UO_2^{2+} Chloride Solutions

Sample	$U–O_{ax}$			$U–O_{eq}$		U–Cl			
UO_2^{2+}	R(Å)[a]	N[b]	σ^2(Å^2)[c]	R	N	R	N	ΔE_0	F-ratio
0 M HCl	1.76	2	0.0018	2.41	5.3	-	-	-10.2	1.0
1 M HCl	1.76	2	0.0016	2.41	5.0	2.71	0.3	-10.8	0.87
2 M HCl	1.75	2	0.0016	2.41	4.8	2.72	0.4	-12.2	0.75
4 M HCl	1.76	2	0.0017	2.41	3.9	2.71	1.0	-11.7	0.43
6 M HCl	1.76	2	0.0015	2.44	3.1	2.72	1.5	-11.5	-
8 M HCl	1.76	2	0.0015	2.48	2.7	2.73	1.8	-10.8	-
10 M HCl	1.76	2	0.0016	2.50	2.5	2.73	2.0	-10.7	-
12 M LiCl	1.77	2	0.0015	2.51	2.2	2.73	2.2	-10.4	-
14 M LiCl	1.77	2	0.0018	2.52	1.9	2.73	2.6	-9.6	-
Dowex/HCl	1.76	2	0.0022	-	-	2.67	4.2	-12.3	1.0
$UO_2Cl_2 \cdot H_2O$[d]	1.72	2	-	2.46	1	2.78	4	-	-
$UO_2(H_2O)_x$[e]	1.70	2	-	2.42	4.9	-	-	-	
$Cs_2UO_2Cl_4$[f]	1.81	2	-	-	-	2.62	4		

a. The standard deviations for R and N as estimated by EXAFSPAK are: $U\text{-}O_{ax}$, R±0.002 Å; $U\text{-}O_{eq}$, R±0.004 Å and N±0.10; U-Cl, R±0.004 Å and N±0.10, respectively.

b. $N = 2$, held constant for $U–O_{ax}$ shell.

c. σ^2 = Debye-Waller factor squared held constant for the additional shells; $U–O_{eq}$, $\sigma^2 = 0.0070$; U–Cl, $\sigma^2 = 0.0050$.

d. XRD, reference 23.

e. XRD, reference 30.

f. XRD, reference 31.

Table 3. EXAFS Structural Parameters for NpO_2^+ Chloride Solutions

Sample	Np–O_{ax}			Np–O_{eq}		Np–Cl			
NpO_2^+	R(Å)[a]	N[b]	σ^2(Å^2)[c]	R	N	R	N	ΔE_0	F-ratio
3 M LiCl	1.85	2	0.0018	2.50	5.0	-	-	-6.7	1.00
4 M LiCl	1.85	2	0.0012	2.52	5.3	-	-	-7.0	1.00
5 M LiCl	1.84	2	0.0010	2.51	5.1	-	-	-7.7	0.95
6 M LiCl	1.83	2	0.0015	2.52	5.0	-	-	-8.5	1.0
7 M LiCl	1.85	2	0.0013	2.53	4.0	2.84	0.7	-7.1	0.37
8 M LiCl	1.84	2	0.0012	2.53	4.0	2.83	0.6	-8.6	0.56
9 M LiCl	1.84	2	0.0018	2.54	3.9	2.85	1.0	-6.9	0.38
10 M LiCl	1.84	2	0.0012	2.53	4.1	2.84	1.0	-6.8	0.34
$CsNpO_2Cl_2 \cdot H_2O$[d]	1.81	2	-	2.49	1	2.86	4	-	-
$NpO_2(H_2O)_x$[e]	1.83	1.6	-	2.52	5.2	-	-	-	

a. The standard deviations for R and N as estimated by EXAFSPAK are: Np-O_{ax}, R±0.003 Å; Np-O_{eq}, R±0.007 Å and N±0.35; Np-Cl, R±0.013 Å and N±0.15, respectively.

b. $N = 2$, held constant for Np–O_{ax} shell.

c. Debye-Waller factor held constant for the additional shells; Np–O_{eq}, $\sigma^2 = 0.0070$; Np–Cl, $\sigma^2 = 0.0050$.

d. XRD, reference 24.

e. EXAFS, reference 33.

Table 4. EXAFS Structural Parameters for Np^{4+} Chloride Solutions

Sample	Ac–O		Ac–Cl			
Np^{4+}	R(Å)	$N^{a,b}$	R	N	ΔE_0	F-ratio
1 M HCl	2.40	11.2	-	-	-8.1	1.0
2 M HCl	2.40	10.9	-	-	-7.8	1.0
3 M HCl	2.41	10.7	-	-	-7.6	1.0
4 M HCl	2.41	10.8	-	-	-7.4	0.94
5 M HCl	2.41	10.3	-	-	-7.2	1.0
6 M HCl	2.42	9.8	2.71	0.6	-7.3	0.81
8 M HCl	2.43	8.7	2.69	1.2	-7.0	0.44
10 M HCl	2.44	7.7	2.69	2.0	-7.2	0.25
Dowex/HCl	-	-	2.61	6.1	-14.1	1.0
$Pu(NO_3)_2(H_20)_x^{2+}$	2.41	11.1[c]				
NpO_2[d]	2.35	8				
Cs_2UCl_6[e]			2.62	6		
Cs_2PuCl_6[f]			2.62	6		

a. The standard deviations for R and N as estimated by EXAFSPAK are: Np-O, R±0.004 Å and N±0.34; Np-Cl, R±0.003 Å and N±0.12, respectively.

b. Debye-Waller factor held constant for the shells;

Np–O, $\sigma^2 = 0.0075$; Np–Cl, $\sigma^2 = 0.0040$.

c. EXAFS, reference 35.

d. XRD, reference 36.

e. XRD, reference 25.

f. XRD, reference 37.

Table 5. EXAFS Structural Parameters for Pu^{3+} Chloride Solutions

Sample	Pu–O (Ln–O)		
Pu^{3+}	R(Å)	$N^{a,b}$	ΔE_0
0.01 M LiCl	2.51	10.2	-10.4
7.0 M LiCl	2.51	8.8	-10.6
8.7 M LiCl	2.51	7.9	-10.0
10.5 M LiCl	2.50	6.6	-8.2
12.3 M LiCl	2.50	5.8	-7.3
$Pr(OH)_3$[c]	2.53	9	
$Nd(NO_3)_3 \cdot 6H_2O$[d]	2.56	10	

a. The standard deviations for R and N as estimated by EXAFSPAK are: Pu-O, R±0.002 Å and N±0.33.

b. σ^2 held constant for Pu–O at 0.0100 $Å^2$.

c. XRD, reference 38

d. XRD, reference 39

Figure Captions

Figure 1 Raw U L_{III}-edge k^3-weighted EXAFS data (A) and corresponding Fourier transforms (B) taken over k=1–13 $Å^{-1}$ for UO_2^{2+} as a function of [Cl^-] and the UO_2^{2+}:Dowex reference. experimental data (—), theoretical fit (····).

Figure 2 Raw Np L_{III}-edge k^3-weighted EXAFS data (A) and corresponding Fourier transforms (B) taken over k=1–12 $Å^{-1}$ for NpO_2^+ as a function of [Cl^-]. experimental data (—), theoretical fit (····).

Figure 3 Curve-fit deconvolution in k-space (A) and R-space (B) for a fit to the Fourier-filtered EXAFS data for NpO_2^+ in 10 M LiCl. The contributions are: Np–O_{ax} (63%), O–Np–O (MS, 5%), Np–O_{eq} (19%), and Np–Cl (13%).

Figure 4 Raw Np L_{III}-edge k^3-weighted EXAFS data (A) and corresponding Fourier transforms (B) taken over k=1–11.5 $Å^{-1}$ for Np^{4+} as a function of [Cl^-] and the Np^{4+}:Dowex reference. experimental data (—), theoretical fit (····).

Figure 5 Raw Pu L_{II}-edge k^3-weighted EXAFS data (A) and corresponding Fourier transforms (B) taken over k=1–9.5 $Å^{-1}$ for Pu^{3+} as a function of [Cl^-]. experimental data (—), theoretical fit (····).

Figure 6 Normalized Actinide $L_{II,III}$-edges. Spectra are presented for Pu^{3+} in 0.01 M LiCl (—),8.7 M LiCl (····), and 12.3 M LiCl (- - -); Np^{4+} in 1.0 M HCl (—), 10 M HCl (····), and Dowex resin (- - -); NpO_2^+ in 3 M LiCl (—) and 10 M LiCl (····); and UO_2^{2+} in 0.0 M HCl (—), 4 M HCl (····), 10 M HCl (- - -), and Dowex resin (—). The U, Np, and Pu data are plotted on a relative energy scale as described in the text. The insert compares the full edges for the respective actinide aquo complexes.

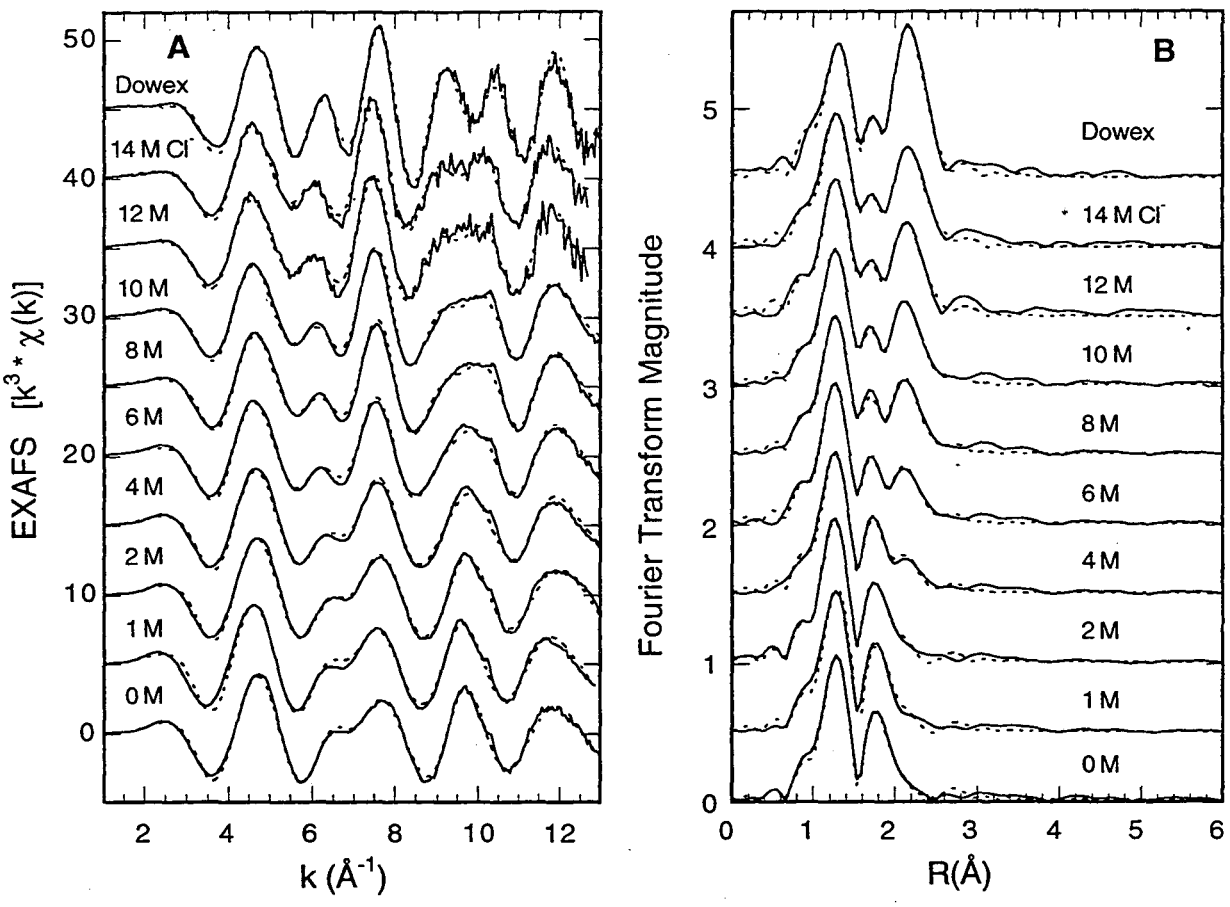
A
Dowex
14 M Cl⁻
12 M
10 M
8 M
6 M
4 M
2 M
1 M
0 M
EXAFS [k³ * χ(k)]
k (Å⁻¹)
B
Dowex
14 M Cl⁻
12 M
10 M
8 M
6 M
4 M
2 M
1 M
0 M
Fourier Transform Magnitude
R(Å)

Figure 1.

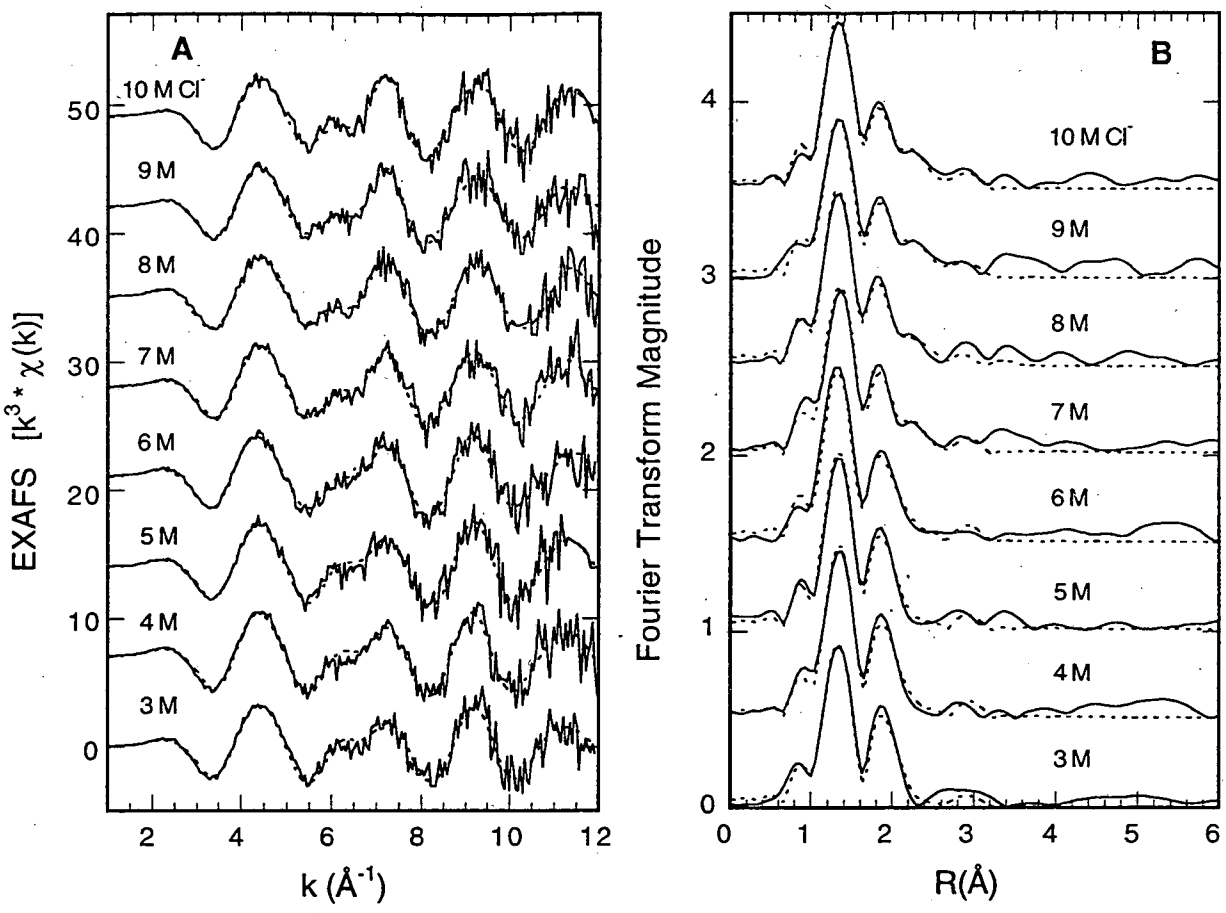
A
10 M Cl⁻
9 M
8 M
7 M
6 M
5 M
4 M
3 M
EXAFS [k³ * χ(k)]
k (Å⁻¹)
B
10 M Cl⁻
9 M
8 M
7 M
6 M
5 M
4 M
3 M
Fourier Transform Magnitude
R(Å)

Figure 2.

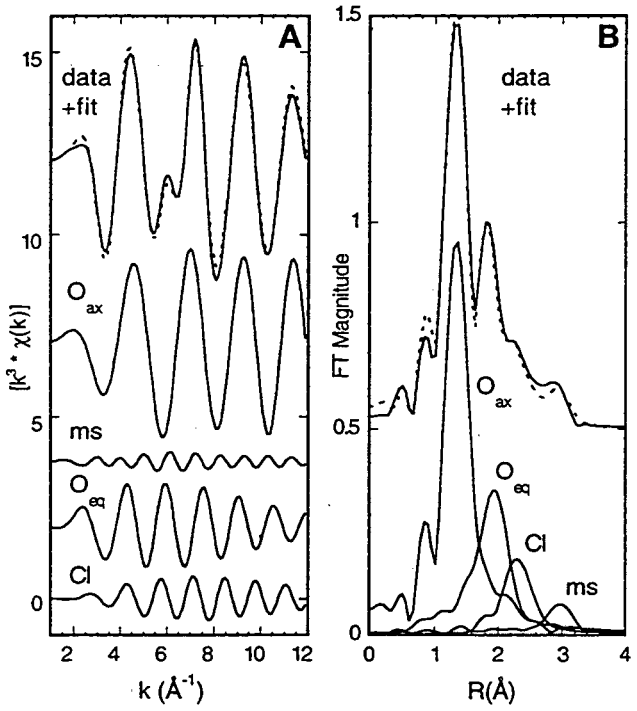

Figure 3.

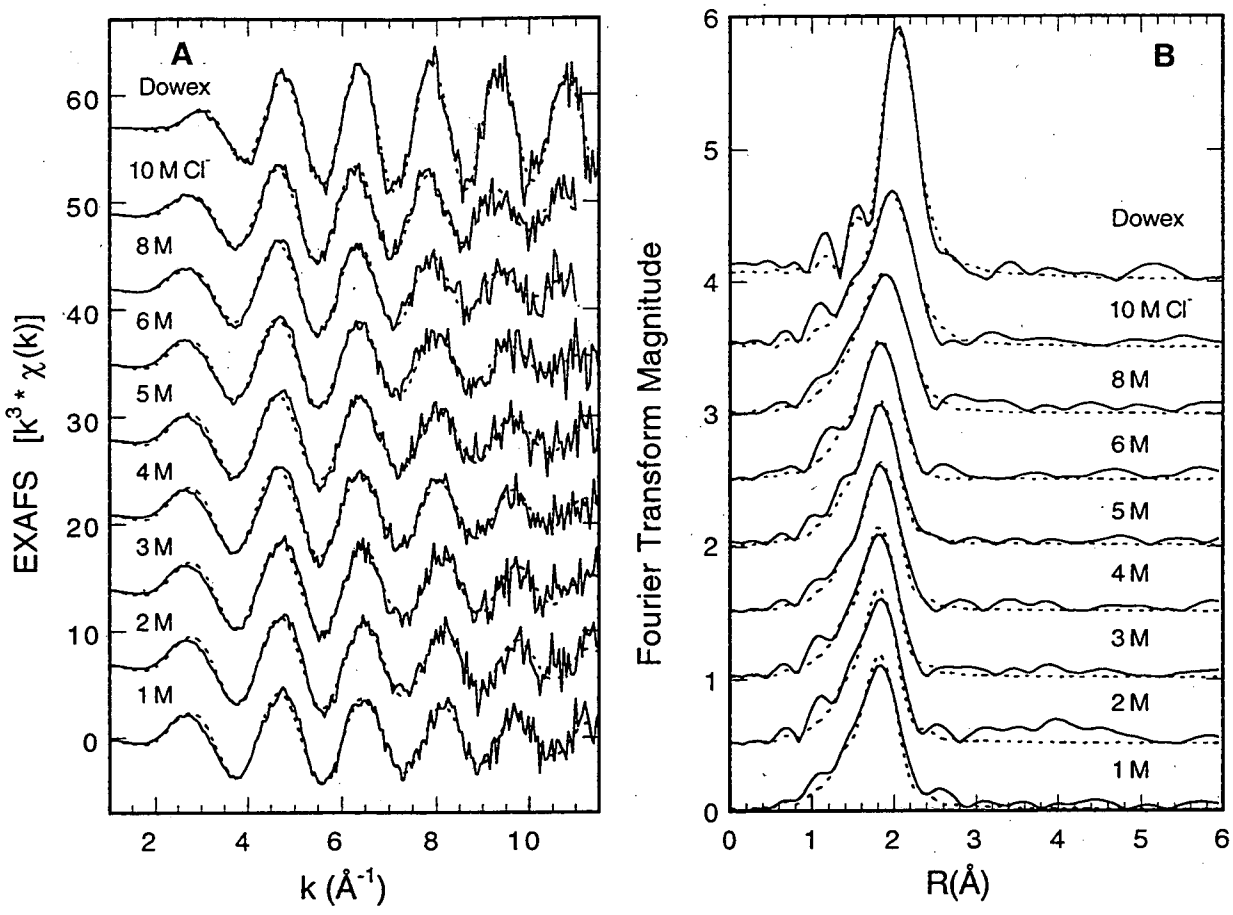
A
Dowex
10 M Cl⁻
8 M
6 M
5 M
4 M
3 M
2 M
1 M
EXAFS [k³ * χ(k)]
k (Å⁻¹)
B
Dowex
10 M Cl⁻
8 M
6 M
5 M
4 M
3 M
2 M
1 M
Fourier Transform Magnitude
R(Å)

Figure 4.

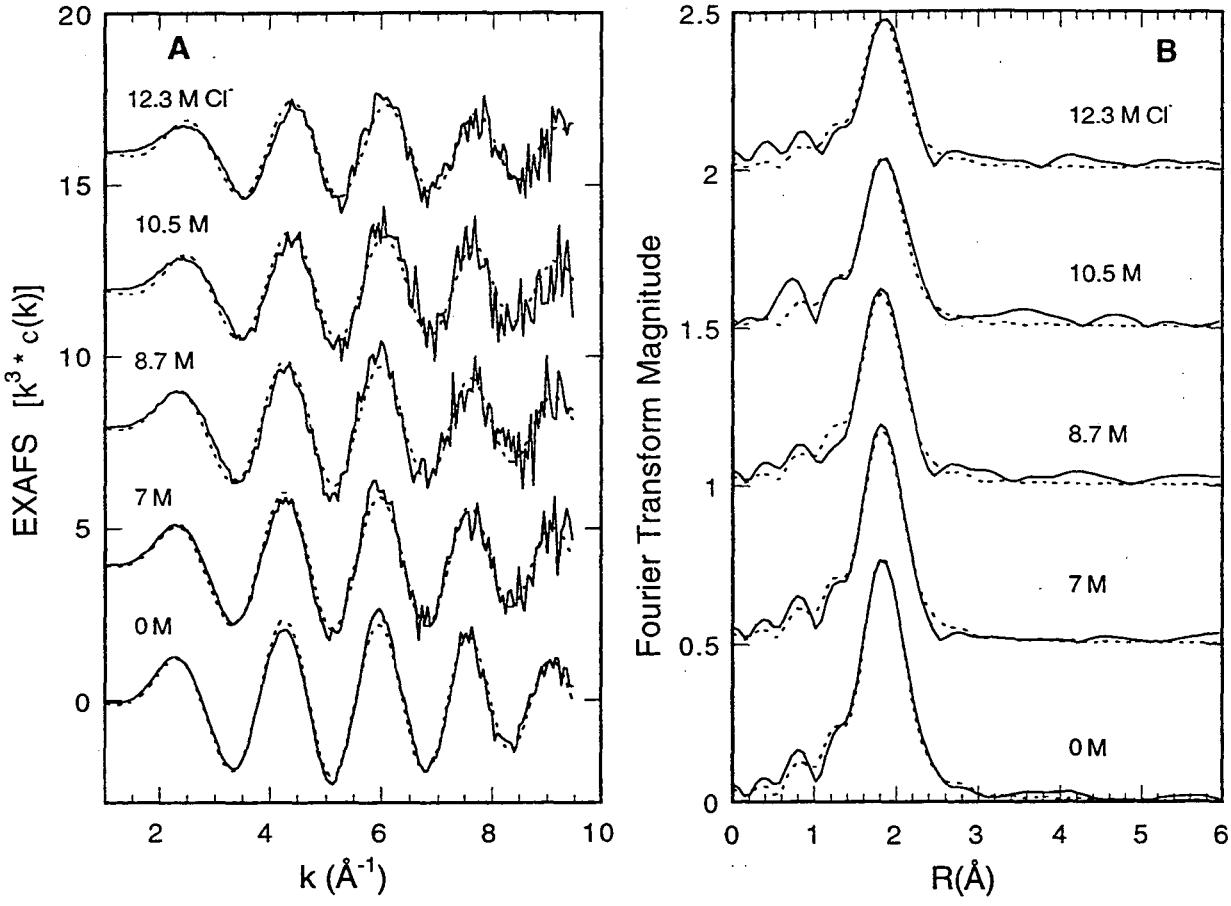
A
12.3 M Cl⁻
10.5 M
8.7 M
7 M
0 M
EXAFS [k³ * c(k)]
k (Å⁻¹)
B
12.3 M Cl⁻
10.5 M
8.7 M
7 M
0 M
Fourier Transform Magnitude
R(Å)

Figure 5.

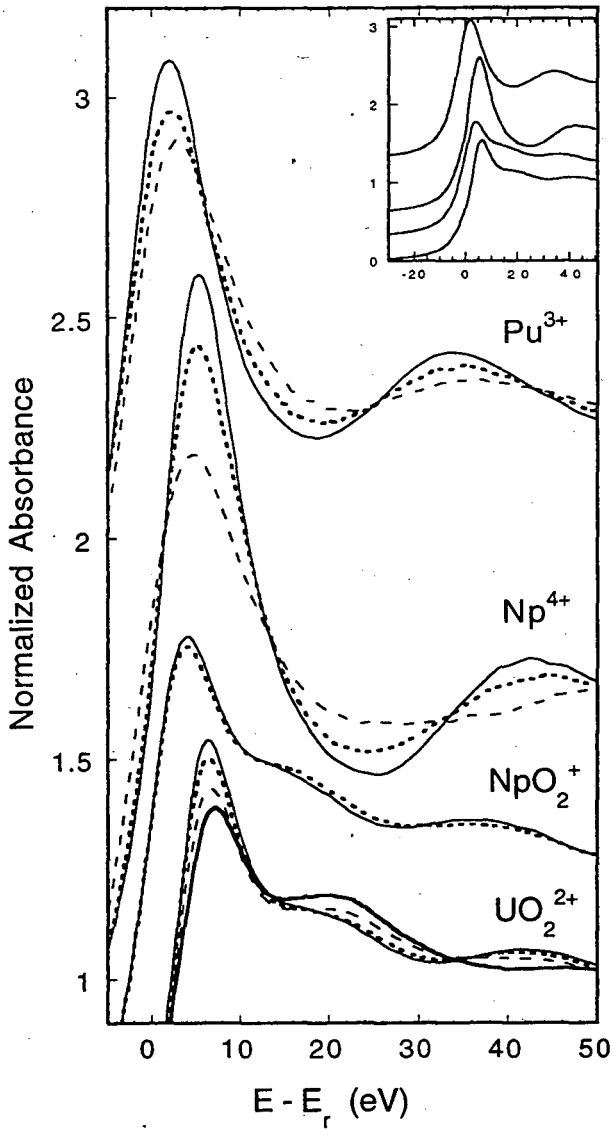

Figure 6.

Ernest Orlando Lawrence Berkeley National Laboratory
One Cyclotron Road ⁞ Berkeley, California 94720

Prepared for the U.S. Department of Energy under Contract No. DE-AC03-76SF00098